Using micro-solvation and generalized coordination numbers to estimate the solvation energies of adsorbed hydroxyl on metal nanoparticles

Hanselman, S.R.; Koper, M.T.M.; Calle Vallejo, F.

PCCP

PAPER

Cite this: *Phys. Chem. Chem. Phys.*, 2023, **25**, 3211

Using micro-solvation and generalized coordination numbers to estimate the solvation energies of adsorbed hydroxyl on metal nanoparticles†

Selwyn Hanselman, [a] Marc T. M. Koper *[a] and Federico Calle-Vallejo *[bcd]

Received 13th October 2022,
Accepted 3rd January 2023

DOI: 10.1039/d2cp04785c

rsc.li/pccp

Solvent-adsorbate interactions have a great impact on catalytic processes in aqueous systems. Implicit solvent calculations are inexpensive but inaccurate toward hydrogen bonds, while a full incorporation of explicit solvation is computationally demanding. Micro-solvation attempts to break this dilemma by including only those solvent molecules directly interacting with the solute and any nearby interfaces, thereby providing a compromise between accuracy and computational expenses. Here, we show that micro-solvation of *OH and its relation to adsorption sites is largely transferable across late transition metal nanoparticles. Solvation energies for *OH on nanoparticles of Ir, Pd, and Pt range from −0.63 ± 0.04 eV to −0.67 ± 0.12 eV, while those on Au and Ag are −0.75 ± 0.07 eV and −1.01 ± 0.05 eV, respectively. These results enable the use of average solvation corrections for *OH on late transition metal nanostructures.

Introduction

Solvation of adsorbed molecular species plays a major yet often neglected role in heterogeneous catalysis in aqueous environments. Indeed, computing adsorbate-solvent interactions is required for highly accurate descriptions of both catalytic intermediates and barriers between them.[1–7] A commonly used approach is implicit solvation, in which bulk properties of the solvent serve as a basis to calculate a continuum response to the solute in the solvent medium.[8,9] Despite being relatively fast and accurate for calculating long-distance solvent–solute interactions, by design implicit solvation methods do not generally take into account volume exclusion and solvent coordination. Previous studies have shown that, specifically, surface solvation effects of water due to hydrogen bonding are greatly underestimated when using implicit methods.[4,10,11] Explicit solvation tackles these issues by including actual water molecules into the simulations, the positions of which can be optimized to obtain possible configurations of all solvent molecules. However, calculating all solvent molecules explicitly (hereafter referred to as "full solvation") requires large numbers of solvent molecules and configurations, which is not always computationally feasible, in particular for nanoparticles.[12,13]

Surface micro-solvation addresses these concerns by substantially reducing the number of explicit solvent molecules, only taking into account those molecules directly solvating the adsorbate, namely, those in the first solvation shell(s). This solvation method models direct species–solvent interactions selectively, which dominate solvation for polar adsorbates in polar and protic solvents.[12,14,15] A previous work compared average solvation energies of *OH and *OOH solvated by 3 water molecules on a series of platinum nanoparticles and surfaces to those solvated by a full monolayer of interfacial H_2O, finding differences within ∼0.05 eV across all adsorption sites and adsorbates.[16] Subsequent work arrived at similar conclusions for Cu(111): the solvation of *OH within a full water bilayer and in the micro-solvation environment with 3 interfacial water molecules differ only by 0.04 eV.[4] Hence, micro-solvation is a promising but still relatively unexplored way to capture hydrogen-bond-dominated interactions between adsorbates and solvents.

In this work, we calculate the formation and solvation energies of *OH on late transition metal nanoparticles of various sizes using density functional theory (DFT), and

[a] *Leiden Institute of Chemistry, Leiden University, P.O. Box 9502, 2300 RA Leiden, The Netherlands. E-mail: m.koper@lic.leidenuniv.nl, federico.calle@ehu.es*
[b] *Nano–Bio Spectroscopy Group and European Theoretical Spectroscopy Facility (ETSF), Department of Polymers and Advanced Materials: Physics, Chemistry and Technology, University of the Basque Country UPV/EHU, Av. Tolosa 72, 20018 San Sebastián, Spain*
[c] *IKERBASQUE, Basque Foundation for Science, Plaza de Euskadi 5, 48009 Bilbao, Spain*
[d] *Department of Materials Science and Chemical Physics & Institute of Theoretical and Computational Chemistry (IQTC), University de Barcelona, Martí i Franquès 1, 08028 Barcelona, Spain*

† Electronic supplementary information (ESI) available. See DOI: https://doi.org/10.1039/d2cp04785c

compare these to each other and to the energies found for Pt in previous work.[16] We find that although the adsorption energies depend on the adsorption site for all metals, most metals show no systematic dependency of solvation energy on *OH adsorption sites. Thus, the solvation energies tend to be consistently constant across adsorption sites for all metals.

Methods

All DFT calculations were performed using VASP 5.4.4, with the spin-restricted PBE exchange–correlation functional, in cubic unit cells using only the Γ-point to sample the *k*-space.[17] We constructed truncated octahedral nanoparticles with 38, 79, and 201 atoms for fcc Ag, Au, Pd, and Ir (the data for Pt were taken from previous work).[16] We adsorbed *OH atop on all the inequivalent sites on those nanoparticles, see Fig. 1. Generalized coordination numbers ($\overline{CN}$) are assigned to each unique adsorption site, following the methodology described in previous work.[18] For a metal site i, $\overline{CN}(i)$ describes the overall coordination of not only the site itself but also its first coordination shell within the nanoparticle, as described in eqn (1).

$$\overline{CN}(i) = \sum_{j=1}^{n_i} \frac{\mathrm{cn}(j)}{\mathrm{cn}_{\max}} \quad (1)$$

Following eqn (1), for each atom closest to the adsorption site within the nanoparticle, we calculated the total number of nearest atoms surrounding it (coordination number, cn(j)), and subsequently divided the sum of these coordination numbers by the maximum coordination number found in the fcc bulk ($\mathrm{cn}_{\max}$, which is equal to 12 for top sites).[18] Note that $\overline{CN}$ can also be defined for bridge and hollow sites by adjusting the value of $\mathrm{cn}_{\max}$,[18] and that tensile and/or compressive strain might also be incorporated in the assessment.[19]

Furthermore, at each adsorption site on each nanoparticle we surrounded *OH by three H_2O molecules, as depicted in Fig. 1, and also added one more H atom to *OH to form a 4-molecule cluster of adsorbed H_2O. By relaxing all atoms in these systems and subsequently obtaining vibrational zero point energies and entropies through single-atom displacements, we calculated formation and solvation energies using the computational hydrogen electrode model (CHE) by Nørskov *et al.*[20] In this model, the target reduction or oxidation reaction occurs against a counter hydrogen oxidation or hydrogen reduction reaction $\frac{1}{2}H_2 \rightleftharpoons H^+ + e^-$, which is assumed to occur without resistance, electrostatic interaction between electrodes, nor with any hydrogen oxidation or reduction overpotential. Effectively, this means that $H^+ + e^-$ can be replaced by $\frac{1}{2}H_2$ in the full chemical reaction. The theory behind and implications of this method have been discussed in several previous works.[21,22] Additionally, the CHE model allows for cancellation of water molecule binding energies in [*OH + 3*H_2O] and [4*H_2O] since it takes the free energies of $H_2(g)$ and the redox partner as a reference. These water molecule binding energies do not affect the solvation energy directly and cancelling them largely eliminates any errors included in these binding energies. The half-reactions for *OH in a micro-solvated environment and *OH in vacuum are shown in eqn (2A) and (3A), respectively. The corresponding free energies are calculated using the CHE as shown in eqn (2B) and (3B), respectively:

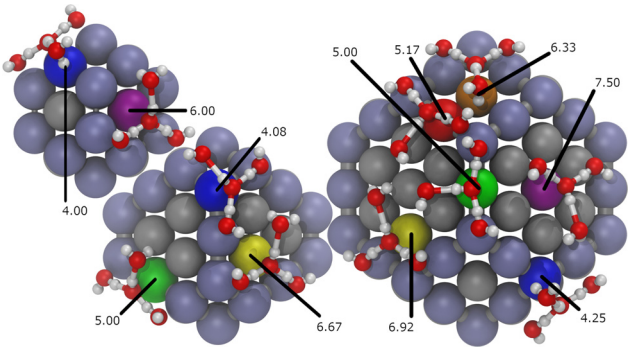

Fig. 1 Metal nanoparticles with 38, 79, and 201 atoms (from left to right) with highlighted adsorption sites and *OH solvated by three water molecules. Labels link adsorption sites to their respective generalized coordination numbers ($\overline{CN}$), as defined in eqn (1).

$$[4^*H_2O] \rightarrow [^*OH + 3^*H_2O] + H^+ + e^- \quad (2A)$$

$$\Delta G_{f,MS} = \Delta G([^*OH + 3^*H_2O]) - \Delta G([4^*H_2O]) + \tfrac{1}{2}\Delta G(H_2(g)) \quad (2B)$$

$$^* + H_2O \rightarrow {}^*OH + H^+ + e^- \quad (3A)$$

$$\Delta G_{f,vac} = \Delta G(^*OH) - \Delta G(H_2O(l)) + \tfrac{1}{2}\Delta G(H_2(g)) \quad (3B)$$

We define the solvation energy of *OH (Ω_{OH}) as the difference between the free energies of eqn (2) and (3):

$$\Omega_{OH} = \Delta G_{f,MS} - \Delta G_{f,vac} \quad (4)$$

Further details, including the formation energy calculation and vibrational calculation methodology, are provided in the ESI,† Sections S.2 and S.3. All errors listed below are mean absolute errors (MAEs). We note that previous works assessed the effect of dispersion corrections at the D3 level in the assessment of adsorbate–solvent interactions. Those works found differences between micro-solvation and solvation approaches based on a water bilayer around 0.05 eV for *OH and *OOH.[4,16] This deviation is smaller than the inherent error for the PBE functional for the assessment of adsorption energies and comparable to the standard deviation of our data from the mean solvation corrections.[23] Hence, in this work we did not include such dispersion corrections (see also the Discussion section). We note, however, that calculations of bulk liquid water using GGA exchange–correlation functionals generally resort to dispersion corrections to address over-structuring and wetting problems, as discussed by Gillan *et al.*[24] Additionally, we performed a spin-unrestricted calculation on a bare Pt_{38} nanoparticle to determine its spin state and hence the validity of our spin-restricted calculations. Since the total spin in such a calculation is zero and the total energy is identical to that of the spin-restricted calculation, we consider spin-restricted

calculations to be sufficiently accurate to simulate *OH–nanoparticle interactions for Pt_{38} and larger particles.

Results

The Pearson correlation coefficients (R) and maximum deviations for scaling relations between formation energies on various metal nanoparticles on individual adsorption sites are listed in Table S5 (ESI†). These Pearson correlation coefficients include information on the sign of the dependency between two datasets, and can be readily converted to the corresponding coefficients of determination R^2. Most correlations of adsorption sites have $R > 0.90$, suggesting similar adsorption properties and, hence, comparable local binding interactions. Several representative correlations are shown in Fig. 2. However, two

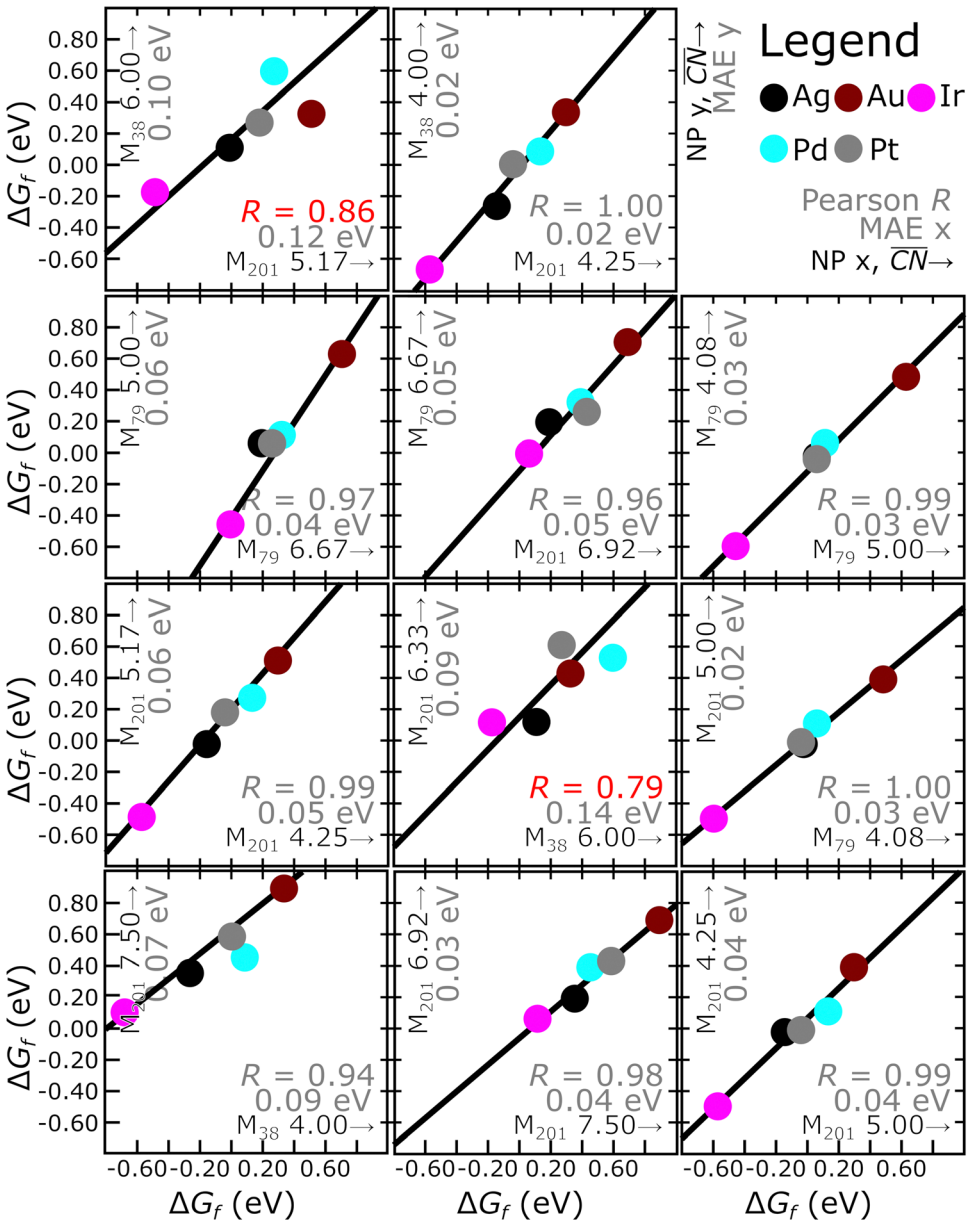

Fig. 2 Selected scaling relations for the formation energies of *OH on all metals in a micro-solvated environment between specific adsorption sites, based on the data listed in Table S2 (ESI†). Linear regressions, correlation coefficients R, and MAEs for either adsorption site involved are listed in Table S5 (ESI†), with corresponding linear fits shown using solid lines. The boxes are sorted by the vertical axes, more specifically the order of the adsorption sites in Tables S2 and S5 (ESI†). Each panel shows the formation energies on all metals for one adsorption site plotted against another. The axes are labeled inside the panel with their respective adsorption sites, M_N representing the N-atom nanoparticle, followed by $\overline{CN}$ of the adsorption site. In the case of the top-left box, formation energies on the $\overline{CN}$ = 5.17 sites on 201-atom nanoparticles are plotted on the horizontal axis, and formation energies on the $\overline{CN}$ = 6.00 sites on 38-atom nanoparticles are plotted on the vertical axis. Pt energies are adapted from previous works.[16] Metals and numbers are denoted as described in the top-right legend.

types of sites show only weak correlations with the other sites: (111) terrace sites on 38-atom nanoparticles, and (100) terrace sites on 201-atom nanoparticles. The former can be attributed to confinement effects and deviation from bulk electronic structures of the small nanoparticles,[25] and the tendency of these nanoparticles to corrugate or even reconstruct in the presence of an adsorbate.[18] The latter was observed earlier on Pt_{201}, and is likely explained by the local environment surrounding the (100) terrace site:[16] solvent water molecules involved in stabilizing *OH are bound strongly by nanoparticle edges, which force the solvent molecules into a strained 90-degree configuration with respect to the adsorbate that cannot be resolved by rotating them. Ag binds *OH on 100 T closely to the trend, and Au even stabilizes it beyond the scaling relation, suggesting they bind water or the adsorbate sufficiently weakly to allow for better solvent coordination with a negligible energy penalty. Note in passing that (100) facets of various transition metals have been reported before to exhibit peculiar adsorption energies and electrocatalytic properties.[26–28] All formation energies on specific adsorption sites, and corresponding linear regressions against adsorption site generalized coordination numbers ($\overline{CN}$) excluding the 38-atom nanoparticle and (100) terrace sites, are shown in Fig. 3. Unless specified otherwise, this set of adsorption sites is used in this work.

Mean formation energies for *OH under vacuum conditions are calculated for each metal across all sites, excluding the 38 atom nanoparticle and 100 terrace sites, as described in the Methods section above using the computational hydrogen electrode.[20] These are in decreasing order: Au (1.33 ± 0.11 eV), Ag (1.06 ± 0.17 eV), Pd (0.90 ± 0.12 eV), Pt (0.81 ± 0.23 eV), and Ir (0.36 ± 0.30 eV). We note that several adsorption sites on different metals were excluded, since no stable top-binding configuration was found. Additionally, previous work on Pt nanoparticles and extended surfaces shows that binding energies using OH(*g*) as a reference are rather exothermic and also scale with $\overline{CN}$, analogous to the correlation between ΔG_{vac} and $\overline{CN}$ found in this work.[18,29] Under micro-solvation, the mean formation energies for *OH are calculated for the same sites as above, as described in the Methods section. These are in decreasing order: Au (0.57 ± 0.18 eV), Pd (0.23 ± 0.12 eV), Pt (0.18 ± 0.21 eV), Ag (0.07 ± 0.11 eV), and Ir (−0.30 ± 0.46 eV). The trend between these formation energies for *OH in vacuum are in line with earlier DFT calculations in which *OH binds most weakly on Ag and Au, and more strongly on Pd, Pt and Ir.[30,31] For micro-solvated *OH on Ag nanoparticles, however, the formation energy is significantly more negative than observed for other transition metal nanoparticles, as shown in Fig. 4. The hydrophobicity of Ag, and to a lesser extent Au, observed for polycrystalline surfaces of respective metals,[32] causes water to bind weakly on nanoparticles of either metal. In the light of energy-decomposition models,[18,33,34] the binding energy of the micro-solvated systems (be them *OH or a central $*H_2O$, both surrounded by 3 peripheral $*H_2O$ molecules) can be decomposed into a sum

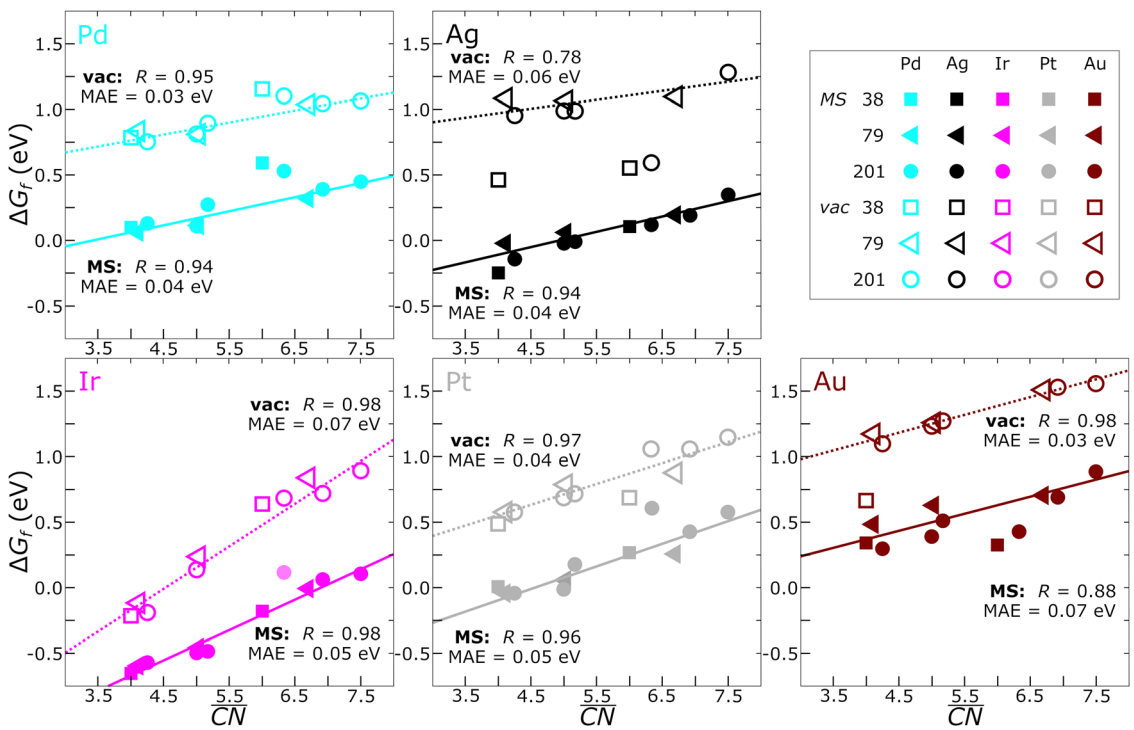

Fig. 3 Formation energies of *OH in micro-solvated (open symbols, from eqn (2)) and vacuum (solid symbols, from eqn (3)) environments as a function of the generalized coordination number ($\overline{CN}$) of the adsorption sites. Pt energies are adapted from previous works.[16] The linear fits are based on 79-atom nanoparticle adsorption sites, and 201-atom nanoparticle adsorption sites excluding the (100) terrace, and the fit qualities and values are listed in Tables S3 and S4 (ESI†), respectively. Colors and shapes are used to represent various metals and nanoparticles as shown in the inset.

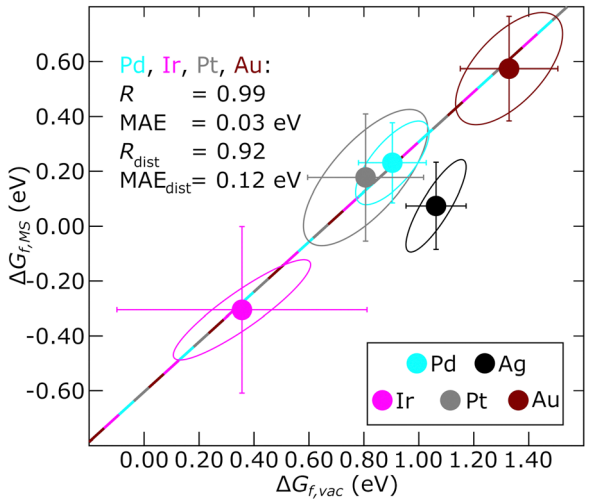

Fig. 4 Comparison of average formation energies of *OH in micro-solvated *versus* vacuum environments across all adsorption sites for various metals. The solid black line (with correlation coefficient R and MAE) is a fit of the mean Gibbs energies for each metal excluding Ag, while R_{dist} is the correlation coefficient for the combined binomial distributions of Gibbs energies for these metals with MAE_{dist}. Multivariate normal distributions for metals are depicted using ellipses corresponding to standard deviations.

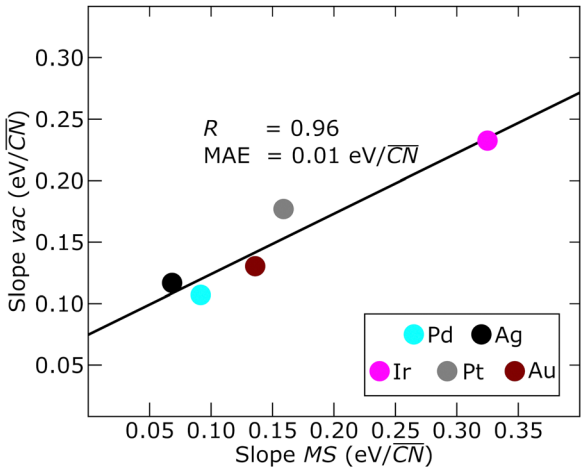

Fig. 5 Comparison of the slopes of *OH formation energies *versus* $\overline{CN}$ in microsolvated *versus* vacuum environments across all adsorption sites for various metals. The solid black line (with correlation coefficient R) is a fit of the slopes per metal.

of different terms accounting for adsorbate–surface interactions, solvent–surface interactions and adsorbate–solvent interactions. For *OH, this is expressed as:

$$\Delta E_{bind}([*OH + 3*H_2O]) = \Delta E_{bind}(*OH) + \Delta E_{bind}(3*H_2O) + \Delta E_{solv} \quad (5)$$

ΔE_{solv} is anticorrelated with $\Delta E_{bind}(3*H_2O)$: given similar $\Delta E_{bind}(*OH)$, when $\Delta E_{bind}(3*H_2O)$ is weaker, adsorbed H_2O is bound less tightly and may move further from its optimum configuration near its binding site with a smaller energy penalty. This means that the solvating water molecules can coordinate better to the solute species, improving ΔE_{solv}. Since *OH is strongly chemisorbed, it can orient itself less freely towards solvating H_2O than free H_2O in the medium, causing the mobility of solvating H_2O to have a greater impact on ΔE_{solv} of *OH than that of free H_2O. This leads to more negative Ω_{OH} as defined in eqn (4).

*OH formation energies in micro-solvated and vacuum configurations correlate strongly with $\overline{CN}$, with $R \geq 0.88$ and average deviations smaller than 0.10 eV for micro-solvated and vacuum configurations on all metals, as shown in Fig. 3 and listed in Table S8 (ESI†). Average deviations with respect to the trend are within the expected accuracy of the PBE functional (no less than 0.10 eV).[35] Conversely, we consider the null hypothesis that formation energies do not fundamentally follow linear trends with respect to coordination numbers, and deviate with respect to the average formation energy. For each metal, average deviations from this null hypothesis, as listed in Table S8 (ESI†), are greater than 0.10 eV. Since deviations relative to the linear regressions are less than half of deviations relative to the null hypothesis, binding energies should scale with $\overline{CN}$. These scaling relations are less correlated with the overall *OH binding energies, in increasing slope order for vacuum *OH: Ag $(0.07\ eV/\overline{CN})$, Pd $(0.09\ eV/\overline{CN})$, Au $(0.14\ eV/\overline{CN})$, Pt $(0.16\ eV/\overline{CN})$, and Ir $(0.32\ eV/\overline{CN})$. This ordering is consistent with the location of the transition metals in the periodic table, with the slope increasing mainly with increasing row numbers in the periodic table, and within rows with decreasing period numbers. When adding micro-solvating water molecules to the nanoparticles, the slopes are in increasing order: Pd $(0.11\ eV/\overline{CN})$, Ag $(0.12\ eV/\overline{CN})$, Au $(0.13\ eV/\overline{CN})$, Pt $(0.17\ eV/\overline{CN})$, and Ir $(0.23\ eV/\overline{CN})$. The slopes for *OH binding energies in vacuum correlate well (R = 0.93) with those with micro-solvation water molecules, as shown in Fig. 5.

The differences between the aforementioned slopes in the micro-solvated and vacuum environments for Pd, Au, and Pt are smaller than $0.03\ eV/\overline{CN}$. This means that the modelled difference in solvation energies between the sites with the lowest (kink sites on 38-atom nanoparticles, $\overline{CN}$ = 3.0) and highest (111 mid-terrace, $\overline{CN}$ = 7.5) generalized coordination numbers is 0.10 eV or smaller, hence within the accuracy of our DFT method. The difference between the micro-solvated and vacuum slopes is affected more strongly on Ag $(+0.05\ eV/\overline{CN})$ and Ir $(-0.09\ eV/\overline{CN})$, which may be related to different solvation physics on these metals, presumably because of their strong micro-solvation energies. In fact, solvation has been shown to affect the slopes of scaling relations among *OH, *OOH and *O on porphyrins.[36]

The micro-solvation energies of *OH on various adsorption sites for different late transition metals are shown in Fig. 6 and tabulated in Table S2 (ESI†). Mean solvation energies (Ω_{OH}) are, in order of increasing strength, Pt (−0.63 ± 0.04 eV), Ir (−0.64 ± 0.12 eV), Pd (−0.67 ± 0.05 eV), Au (−0.75 ± 0.07 eV), and Ag

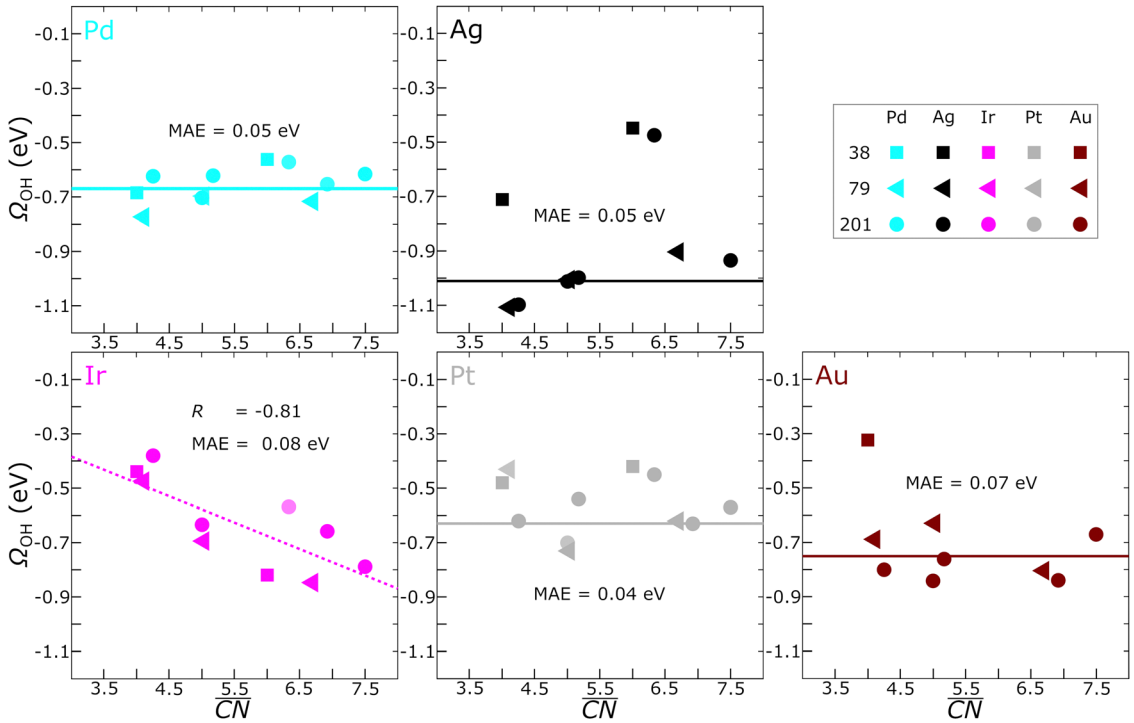

Fig. 6 Solvation energies of *OH (Ω_{OH}, eqn (4)) as a function of the $\overline{CN}$ of the adsorption sites. The linear fit for Ir (dotted line) and mean solvation energies (solid lines) for the other metals are based on 79-atom nanoparticle adsorption sites, and 201-atom nanoparticle adsorption sites excluding the (100) terrace, only including sites on nanoparticles for which top-binding vacuum configurations exist, as shown in Table S8 (ESI†). Fit values and qualities are listed in Tables S7 and S8 (ESI†), respectively. Colors and shapes are used to represent different metals and nanoparticles, respectively, as listed in the inset.

(-1.01 ± 0.05 eV). These values are mostly in line with earlier (111) slab calculations on Pt alloys solvated with a water bilayer by Granda-Marulanda *et al.*,[37] although the corrections for Au and Ag obtained in this study are considerably more negative. We attribute the departures for Ag and Au to the relatively weakly-bound near-surface H_2O. In addition, Tripkovic lists hydrogen bond energies (ΔE_{HB}(OH)) for *OH on Ag(111), Pd(111), and Pt(111), which are defined similarly but not identically from the solvation energies in this study.[7] Notwithstanding the fundamental differences (*i.e.*, a free energy change *vs.* a DFT energy change), Pd(111) and Pt(111) have similar hydrogen bond energies as in our calculations, while Ag(111) is solvated less strongly than expected from our calculations probably due to a shift in vacuum *OH binding site from on-top to bridge and the different exchange–correlation functional (RPBE) used by Tripkovic.

Excluding Ir, the average deviations for individual solvation energies are below 0.10 eV for all metals, while maximum deviations are no greater than 0.13 eV (for Au), as listed in Table S9 (ESI†). Hence, for most metals (Ag, Au, Pt and Pd) an average solvation energy rather than a scaling relation as a function of $\overline{CN}$ suffices to describe solvation, which generalizes previous observations for Pt nanoparticles[16] to a variety of transition metals. If additional accuracy is needed, a linear fit might be used for Ag, with correlation coefficient $R = 0.91$, and a mean absolute difference from the fit of 0.03 *versus* 0.05 eV from the average solvation energy. By contrast, Ir shows an average individual solvation energy deviation of 0.12 eV with respect to the mean value, and a maximum deviation of 0.26 eV. With respect to the linear regression for Ir solvation energies *versus* $\overline{CN}$ ($R = -0.81$), the mean deviation is 0.08 eV while the maximum deviation is 0.12 eV. Hence, *OH formation energies under micro-solvation are not randomly scattered around the mean value, and rather seem to be anticorrelated with $\overline{CN}$, with a slope of $-0.10\,\text{eV}/\overline{CN}$.

To elucidate the physical effects causing the difference between Ir and the other metals, we need to decompose the solvation energies (eqn (4)) into the formation energies of surface (adsorbate–water) complexes and *OH in vacuum:

$$\Omega_{OH} = \Delta G_{f,MS} - \Delta G_{f,vac} = \Delta G_{f,[*OH\,+\,3*H_2O]} - \Delta G_{f,[4*H_2O]} - \Delta G_{f,vac} \quad (6)$$

Although $\Delta G_{f,MS}$ scales with $\overline{CN}$, neither $\Delta G_{f,[*OH\,+\,3*H_2O]}$, nor $\Delta G_{f,[4*H_2O]}$ appear to depend linearly on it. The formation energies of these surface complexes for individual metals correlate well with each other ($R > 0.80$), as shown in Table S9 (ESI†). It is known that shared adsorption mechanisms and associated bond orders cause scaling relations to appear between different adsorbates for equal combinations of metals and adsorption sites.[31,38,39] In this case, assuming that the dependency of formation energies on $\overline{CN}$ is similar across adsorption sites, supported by the correlations described above, we find scaling relations for $\Delta G_{f,[*OH\,+\,3*H_2O]}$ between metals and for $\Delta G_{f,[4*H_2O]}$ between metals, the slopes of which (listed in Table S10, ESI†) represent ratios of adsorbate–surface

Table 1 Comparison between different approaches for the assessment of the number of hydrogen bonds made between *OH and water, and the solvation correction for *OH. AIMD: *ab initio* molecular dynamics. MS: micro-solvation. Bilayer: a periodic ice-like water layer above the surface

	Number of hydrogen bonds		Ω_{OH} (eV)		
Metal	AIMD	MS (this work)	AIMD	Bilayer	MS (this work)
Pt	2.76 ± 0.07[40]	3	−0.58 ± 0.07[40]	−0.57,[37] −0.58[3]	−0.63 ± 0.04
Au	2.96 ± 0.02[40]	3	−0.68 ± 0.08[40]	−0.68 (this work)	−0.75 ± 0.07

bond strengths. For most metals, $\Delta G_{f,[4*H_2O]}$ depends only weakly on $\overline{CN}$, and its averages range from ∼0.5 to 0.8 eV with respect to bulk water. However, $\Delta G_{f,[4*H_2O]}$ on Ir is less positive (on average ∼ + 0.2 eV), and based on the slopes of scaling relations between $\Delta G_{f,[4*H_2O]}$ for individual metals, depends 1.87 to 2.75 times as strongly on $\overline{CN}$ compared to the other metals. Similarly, $\Delta G_{f,[*OH + 3*H_2O]}$ depends 1.95 to 2.35 times as strongly on $\overline{CN}$ on Ir compared to the other metals. However, the slopes between $\Delta G_{f,vac}$ on Ir *versus* other metals range from 2.37 to 3.26, and are 22–54% higher than their respective slopes between $\Delta G_{f,[*OH + 3*H_2O]}$. This uniform weakening of the bond strength of [*OH + 3*H_2O] to the nanoparticle compared to vacuum *OH adsorption is displayed by Ir, yet not observed on Ag, Au or Pd. Combined with the observation that formation energies scale with $\overline{CN}$ on all metals and most strongly on Ir, this explains the negative slope of Ω_{OH} on Ir with respect to $\overline{CN}$.

To numerically substantiate the analysis of eqn (6), consider the cases of iridium and palladium. According to Tables S4 and S9 (ESI†), for Ir we have: $\Delta G_{f,[*OH+3*H_2O]} = 0.34\overline{CN} - 1.98$, $\Delta G_{f,[4*H_2O]} = 0.10\overline{CN} - 0.38$, and $\Delta G_{f,vac} = 0.32\overline{CN} - 1.47$. As a result, eqn 6 applied to Ir gives: $\Omega_{OH} = -0.09\overline{CN} - 0.13$. On the other hand, following Tables S4 and S9 (ESI†), for Pd we have: $\Delta G_{f,[*OH+3*H_2O]} = 0.14\overline{CN} - 0.04$, $\Delta G_{f,[4*H_2O]} = 0.03\overline{CN} + 0.33$, and $\Delta G_{f,vac} = 0.09\overline{CN} + 0.39$. Accordingly, eqn 6 gives for Pd: $\Omega_{OH} = 0.02\overline{CN} - 0.70$. Thus, in agreement with Fig. 6, from this brief analysis we conclude that Ω_{OH} for Ir sites is a linear function of $\overline{CN}$ with a negative slope, whereas Ω_{OH} for Pd does not depend strongly on $\overline{CN}$ and is close to −0.70 eV. Note in passing that the resulting equations are commensurate to the parameters in Table S7, which were obtained by linear regression. The differences stem from the fair correlation coefficients obtained when correlating $\Delta G_{f,[*OH+3*H_2O]}$ and $\Delta G_{f,[4*H_2O]}$ with $\overline{CN}$.

Finally, analysis of bond lengths, as shown in Table S11 (ESI†), shows a highly consistent O–H bond length in *OH between metals of 0.976 ± 0.001 Å to 0.979 ± 0.001 Å, in which the error bars correspond to average deviations for the specific metal. Adding micro-solvation water molecules causes an increase in the O–H bond length in *OH for Ir by 0.023 ± 0.003 Å (2.3 ± 0.8%), whereas Ag shows an increase of 0.007 ± 0.003 Å (0.7 ± 0.3%), Au 0.011 ± 0.003 Å (2.3 ± 0.3%), and Pd 0.013 ± 0.007 Å (1.4 ± 0.7%). This coincides with a shorter hydrogen bond distance from H in *OH in Ir, which is 1.775 ± 0.105 Å, *versus* Ag at 2.016 ± 0.092 Å, Au at 1.913 ± 0.047 Å, and Pd at 1.858 ± 0.108 Å. Similar trends, though less pronounced, are visible for micro-solvated H_2O, which shows longer O–H bonds relative to micro-solvated *OH across all metals.

Discussion

Ir compared to the other metals. However, in our dataset for which *OH solvation energies noticeably depend on $\overline{CN}$. As calculating several nanoparticles for the full set of transition metals is out of the scope of this work, we cannot determine whether Ir is an exception or part of a trend. However, there is a difference in adsorption energy slopes between vacuum and micro-solvated *OH on Ir that is not observed for the other metals. Moreover, we found additional differences in water binding energies and adsorbate bond lengths for Ir with respect to the other metals. These differences suggest that water is bound more strongly on Ir, which directly causes solvation energies not to be constant. We expect that this behavior applies to all transition metals that bind water strongly. This opens up opportunities for further research on nanoparticles of early transition metals.

Furthermore, solvation corrections for *OH obtained *via* micro-solvation by three water molecules have been shown before to compare well to those obtained from a water bilayer.[3,4] If these bilayer solvation corrections in turn agree with the solvation corrections obtained *via ab initio* molecular dynamics (AIMD), this by extension lends more credence to the accuracy of micro-solvation. The results in Table 1 suggest that a water bilayer suffices to capture the energetics of solvation at metal surfaces. Indeed, the solvation energy of *OH on Pt(111) was found to be −0.57 eV using a static bilayer,[37] and −0.58 ± 0.07 eV by means of AIMD calculations,[40] both calculated with RPBE-D3. The static bilayer with PBE also gives Ω_{OH} = −0.58 eV,[3] and in this study we found an average solvation correction of −0.63 ± 0.04 eV for *OH on Pt nanoparticles with PBE.

In addition, the average solvation energy of *OH on Au found in this study is −0.75 ± 0.07 eV, which is close to the value of −0.68 ± 0.08 eV obtained by means of AIMD,[40] and to the value of −0.68 eV obtained using a water bilayer (see Section S.8, ESI†). Furthermore, the average number of hydrogen bonds for *OH in a bilayer and in our micro-solvation approach is 3, which is close to the average values of 2.76 ± 0.07 and 2.96 ± 0.02 bonds found using AIMD for Pt(111) and Au(111). Altogether, these observations support the idea that, in spite of their simplicity, a water bilayer and micro-solvation with 3 water molecules both seem to capture the essence of *OH solvation on transition metals.

Conclusions

Adsorbate-solvent interactions are of great importance for catalytic processes in aqueous media, and micro-solvation provides a promising means of efficiently and inexpensively capturing these interactions in computations. In this work, we

have shown that the trends in and averages of micro-solvation energies for *OH on nanoparticles are comparable for several late transition metals. Crucially, for Ag, Au, Pd and Pt the solvation energy can be considered independent of local nanoparticle geometry for sufficiently large nanoparticles and extended surfaces, especially when the sites display hexagonal symmetry.

Average solvation corrections are larger (*i.e.*, more negative) for weakly binding metals such as Ag and Au, compared to other late transition metals. For strongly binding metals such as Ir, hydrogen bonds from strongly bound water molecules weaken the *OH–nanoparticle bond and, thus, solvation energies scale linearly with the coordination of the adsorption sites.

In broad terms, we found *via* micro-solvation that *OH–water interactions are generally constant on nanoparticles of a given late transition metal, regardless of the coordination of the adsorption sites. When *OH–water interactions are not constant, generalized coordination numbers may be used to rationalize the trends.

Conflicts of interest

The authors declare no competing financial interests.

Acknowledgements

This work was partially supported by the Netherlands Organization for Scientific Research (NWO) in the framework of the Solar Fuels Graduate Program. The grants RYC-2015-18996, MDM-2017-0767, PID2021-127957NB-I00 and RTI2018-095460-*B*-I00 were funded by MCIN/AEI/10.13039/501100011033 and by the European Union. This research was also partly funded by Generalitat de Catalunya 2017SGR13. The work has been performed under the Project HPC-EUROPA3 (INFRAIA-2016-1-730897), with the support of the EC Research Innovation Action under the H2020 Programme; in particular, SH gratefully acknowledges the support of IQTCUB and the computer resources and technical support provided by BSC. The use of supercomputing facilities at SURFsara was sponsored by NWO Physical Sciences, with financial support by NWO.

References

1 M. Van den Bossche, E. Skúlason, C. Rose-Petruck and H. Jónsson, Assessment of Constant-Potential Implicit Solvation Calculations of Electrochemical Energy Barriers for H2 Evolution on Pt, *J. Phys. Chem. C*, 2019, **123**(7), 4116–4124, DOI: **10.1021/acs.jpcc.8b10046**.

2 H.-J. Chun, V. Apaja, A. Clayborne, K. Honkala and J. Greeley, Atomistic Insights into Nitrogen-Cycle Electrochemistry: A Combined DFT and Kinetic Monte Carlo Analysis of NO Electrochemical Reduction on Pt(100), *ACS Catal.*, 2017, **7**(6), 3869–3882, DOI: **10.1021/acscatal.7b00547**.

3 Z.-D. He, S. Hanselman, Y.-X. Chen, M. T. M. Koper and F. Calle-Vallejo, Importance of Solvation for the Accurate Prediction of Oxygen Reduction Activities of Pt-Based Electrocatalysts, *J. Phys. Chem. Lett.*, 2017, **8**(10), 2243–2246, DOI: **10.1021/acs.jpclett.7b01018**.

4 A. Rendón-Calle, S. Builes and F. Calle-Vallejo, Substantial Improvement of Electrocatalytic Predictions by Systematic Assessment of Solvent Effects on Adsorption Energies, *Appl. Catal., B*, 2020, **276**, 119147, DOI: **10.1016/j.apcatb.2020.119147**.

5 S. Sakong and A. Groß, The Importance of the Electrochemical Environment in the Electro-Oxidation of Methanol on Pt(111), *ACS Catal.*, 2016, **6**(8), 5575–5586, DOI: **10.1021/acscatal.6b00931**.

6 S. A. Akhade, W. Luo, X. Nie, A. Asthagiri and M. J. Janik, Theoretical Insight on Reactivity Trends in CO2 Electroreduction across Transition Metals, *Catal. Sci. Technol.*, 2016, **6**(4), 1042–1053, DOI: **10.1039/C5CY01339A**.

7 V. Tripkovic, Thermodynamic Assessment of the Oxygen Reduction Activity in Aqueous Solutions, *Phys. Chem. Chem. Phys.*, 2017, **19**(43), 29381–29388, DOI: **10.1039/C7CP05448C**.

8 J. Ho, M. L. Coote, C. Cramer and D. G. Truhlar, Theoretical Calculation of Reduction Potentials, *Organic Electrochemistry*, CRC Press, 5th edn, 2015, pp. 229–260.

9 K. Mathew, V. S. C. Kolluru, S. Mula, S. N. Steinmann and R. G. Hennig, Implicit Self-Consistent Electrolyte Model in Plane-Wave Density-Functional Theory, *J. Chem. Phys.*, 2019, **151**(23), 234101, DOI: **10.1063/1.5132354**.

10 Q. Zhang and A. Asthagiri, Solvation Effects on DFT Predictions of ORR Activity on Metal Surfaces, *Catal. Today*, 2019, **323**, 35–43, DOI: **10.1016/j.cattod.2018.07.036**.

11 C. M. Gray, K. Saravanan, G. Wang and J. A. Keith, Quantifying Solvation Energies at Solid/Liquid Interfaces Using Continuum Solvation Methods, *Mol. Simul.*, 2017, **43**(5–6), 420–427, DOI: **10.1080/08927022.2016.1273525**.

12 R. F. de Morais, T. Kerber, F. Calle-Vallejo, P. Sautet and D. Loffreda, Capturing Solvation Effects at a Liquid/Nanoparticle Interface by Ab Initio Molecular Dynamics: Pt201 Immersed in Water, *Small*, 2016, **12**(38), 5312–5319, DOI: **10.1002/smll.201601307**.

13 Y. Basdogan, A. M. Maldonado and J. A. Keith, Advances and Challenges in Modeling Solvated Reaction Mechanisms for Renewable Fuels and Chemicals, *Wiley Interdiscip. Rev.: Comput. Mol. Sci.*, 2020, **10**(2), e1446, DOI: **10.1002/wcms.1446**.

14 X. Zhang, R. S. DeFever, S. Sarupria and R. B. Getman, Free Energies of Catalytic Species Adsorbed to Pt(111) Surfaces under Liquid Solvent Calculated Using Classical and Quantum Approaches, *J. Chem. Inf. Model.*, 2019, **59**(5), 2190–2198, DOI: **10.1021/acs.jcim.9b00089**.

15 C.-H. Chan, F. Poignant, M. Beuve, E. Dumont and D. Loffreda, A Water Solvation Shell Can Transform Gold Metastable Nanoparticles in the Fluxional Regime, *J. Phys. Chem. Lett.*, 2019, **10**(5), 1092–1098, DOI: **10.1021/acs.jpclett.8b03822**.

16 F. Calle-Vallejo, R. F. de Morais, F. Illas, D. Loffreda and P. Sautet, Affordable Estimation of Solvation Contributions to the Adsorption Energies of Oxygenates on Metal Nanoparticles, *J. Phys. Chem. C*, 2019, **123**(9), 5578–5582, DOI: **10.1021/acs.jpcc.9b01211**.

17 J. P. Perdew, K. Burke and M. Ernzerhof, Generalized Gradient Approximation Made Simple, *Phys. Rev. Lett.*, 1996, **77**(18), 3865–3868, DOI: **10.1103/PhysRevLett.77.3865**.

18 F. Calle-Vallejo, P. Sautet and D. Loffreda, Understanding Adsorption-Induced Effects on Platinum Nanoparticles: An Energy-Decomposition Analysis, *J. Phys. Chem. Lett.*, 2014, **5**(18), 3120–3124, DOI: **10.1021/jz501263e**.

19 F. Calle-Vallejo and A. S. Bandarenka, Enabling Generalized Coordination Numbers to Describe Strain Effects, *ChemSusChem*, 2018, **11**(11), 1824–1828, DOI: **10.1002/cssc.201800569**.

20 J. K. Nørskov, J. Rossmeisl, A. Logadottir, L. Lindqvist, J. R. Kitchin, T. Bligaard and H. Jónsson, Origin of the Overpotential for Oxygen Reduction at a Fuel-Cell Cathode, *J. Phys. Chem. B*, 2004, **108**(46), 17886–17892, DOI: **10.1021/jp047349j**.

21 J. Rossmeisl, K. Chan, R. Ahmed, V. Tripković and M. E. Björketun, *p*H in Atomic Scale Simulations of Electrochemical Interfaces, *Phys. Chem. Chem. Phys.*, 2013, **15**(25), 10321–10325, DOI: **10.1039/C3CP51083B**.

22 F. Calle-Vallejo and M. T. M. Koper, First-Principles Computational Electrochemistry: Achievements and Challenges, *Electrochim. Acta*, 2012, **84**, 3–11, DOI: **10.1016/j.electacta.2012.04.062**.

23 J. Wellendorff, T. L. Silbaugh, D. Garcia-Pintos, J. K. Nørskov, T. Bligaard, F. Studt and C. T. Campbell, A Benchmark Database for Adsorption Bond Energies to Transition Metal Surfaces and Comparison to Selected DFT Functionals, *Surf. Sci.*, 2015, **640**, 36–44, DOI: **10.1016/j.susc.2015.03.023**.

24 M. J. Gillan, D. Alfè and A. Michaelides, Perspective: How Good Is DFT for Water, *J. Chem. Phys.*, 2016, **144**(13), 130901, DOI: **10.1063/1.4944633**.

25 F. Viñes, J. R. B. Gomes and F. Illas, Understanding the Reactivity of Metallic Nanoparticles: Beyond the Extended Surface Model for Catalysis, *Chem. Soc. Rev.*, 2014, **43**(14), 4922–4939, DOI: **10.1039/C3CS60421G**.

26 R. R. Adić, N. M. Marković and V. B. Vešović, Structural Effects in Electrocatalysis: Oxygen Reduction on the Au (100) Single Crystal Electrode, *J. Electroanal. Chem. Interfacial Electrochem.*, 1984, **165**(1), 105–120, DOI: **10.1016/S0022-0728(84)80090-X**.

27 F. J. Vidal-Iglesias, N. Garcia-Araez, V. Montiel, J. M. Feliu and A. Aldaz, Selective Electrocatalysis of Ammonia Oxidation on Pt(100) Sites in Alkaline Medium, *Electrochem. Commun.*, 2003, **5**(1), 22–26, DOI: **10.1016/S1388-2481(02)00521-0**.

28 H. Li, F. Calle-Vallejo, M. J. Kolb, Y. Kwon, Y. Li and M. T. M. Koper, Why (1 0 0) Terraces Break and Make Bonds: Oxidation of Dimethyl Ether on Platinum Single-Crystal Electrodes, *J. Am. Chem. Soc.*, 2013, **135**(38), 14329–14338, DOI: **10.1021/ja406655q**.

29 F. Calle-Vallejo, J. I. Martínez, J. M. García-Lastra, P. Sautet and D. Loffreda, Fast Prediction of Adsorption Properties for Platinum Nanocatalysts with Generalized Coordination Numbers, *Angew. Chem., Int. Ed.*, 2014, **53**(32), 8316–8319, DOI: **10.1002/anie.201402958**.

30 V. Viswanathan, H. A. Hansen, J. Rossmeisl and J. K. Nørskov, Universality in Oxygen Reduction Electrocatalysis on Metal Surfaces, *ACS Catal.*, 2012, **2**(8), 1654–1660, DOI: **10.1021/cs300227s**.

31 F. Calle-Vallejo, D. Loffreda, M. T. M. Koper and P. Sautet, Introducing Structural Sensitivity into Adsorption–Energy Scaling Relations by Means of Coordination Numbers, *Nat. Chem.*, 2015, **7**(5), 403–410, DOI: **10.1038/nchem.2226**.

32 G. Valette, Hydrophilicity of Metal Surfaces: Silver, Gold and Copper Electrodes, *J. Electroanal. Chem. Interfacial Electrochem.*, 1982, **139**(2), 285–301, DOI: **10.1016/0022-0728(82)85127-9**.

33 C. Dupont, Y. Jugnet and D. Loffreda, Theoretical Evidence of PtSn Alloy Efficiency for CO Oxidation, *J. Am. Chem. Soc.*, 2006, **128**(28), 9129–9136, DOI: **10.1021/ja061303h**.

34 K. Kitaura and K. Morokuma, A New Energy Decomposition Scheme for Molecular Interactions within the Hartree-Fock Approximation, *Int. J. Quantum Chem.*, 1976, **10**(2), 325–340, DOI: **10.1002/qua.560100211**.

35 R. Peverati and D. G. Truhlar, Quest for a Universal Density Functional: The Accuracy of Density Functionals across a Broad Spectrum of Databases in Chemistry and Physics, *Philos. Trans. R. Soc., A*, 2011, **2014**(372), 20120476, DOI: **10.1098/rsta.2012.0476**.

36 F. Calle-Vallejo, A. Krabbe and J. M. García-Lastra, How Covalence Breaks Adsorption-Energy Scaling Relations and Solvation Restores Them, *Chem. Sci.*, 2016, **8**(1), 124–130, DOI: **10.1039/C6SC02123A**.

37 L. P. Granda-Marulanda, S. Builes, M. T. M. Koper and F. Calle-Vallejo, Influence of van der Waals Interactions on the Solvation Energies of Adsorbates at Pt-Based Electrocatalysts, *ChemPhysChem.*, 2019, **20**(22), 2968–2972, DOI: **10.1002/cphc.201900512**.

38 F. Abild-Pedersen, J. Greeley, F. Studt, J. Rossmeisl, T. R. Munter, P. G. Moses, E. Skúlason, T. Bligaard and J. K. Nørskov, Scaling Properties of Adsorption Energies for Hydrogen-Containing Molecules on Transition-Metal Surfaces, *Phys. Rev. Lett.*, 2007, **99**(1), 016105, DOI: **10.1103/PhysRevLett.99.016105**.

39 F. Calle-Vallejo, J. I. Martínez, J. M. García-Lastra, J. Rossmeisl and M. T. M. Koper, Physical and Chemical Nature of the Scaling Relations between Adsorption Energies of Atoms on Metal Surfaces, *Phys. Rev. Lett.*, 2012, **108**(11), 116103, DOI: **10.1103/PhysRevLett.108.116103**.

40 H. H. Heenen, J. A. Gauthier, H. H. Kristoffersen, T. Ludwig and K. Chan, Solvation at Metal/Water Interfaces: An Ab Initio Molecular Dynamics Benchmark of Common Computational Approaches, *J. Chem. Phys.*, 2020, **152**(14), 144703, DOI: **10.1063/1.5144912**.